MTLA 30 (2023) 101825

Contents lists available at ScienceDirect

Materialia

journal homepage: www.elsevier.com/locate/mtla

Full Length Article

Optical coherence tomography (OCT) for the analysis of zirconia crystalline phase transformation

Anelyse Arata Found [a,b,*], L.R. De Pretto [a], V. Ussui [a,1], N.B. Lima [a], G.M. De Souza [c], J.P.B. Machado [d], R.N. Tango [e], A.Z. Freitas [f], D.R.R. Lazar [a]

[a] Nuclear and Energy Research Institute IPEN-CNEN/SP, Cidade Universitária "Armando de Salles Oliveira", 2242 Prof. Lineu Prestes Avenue, São Paulo, SP, 05508-900, Brazil
[b] Division of Restorative Dentistry, Schulich School of Medicine and Dentistry, The University of Western Ontario, London, ON, Canada
[c] Faculty of Medicine and Dentistry, University of Toronto, 124 Edward St, Toronto, ON, Toronto, ON M5G 1G6, Canada
[d] Associated Laboratory for Sensors and Materials, National Institute for Space Research INPE, 1758 Astronautas Avenue, Jardim da Granja, São José dos Campos, SP 12227-010, Brazil
[e] Department of Dental Materials and Prosthodontics, UNESP, Sao Paulo State University - Institute of Science and Technology, 777 Eng. Francisco José Longo Avenue, Jardim São Dimas, São José dos Campos, SP 12245-000, Brazil
[f] Center for Lasers and Applications, Nuclear and Energy Research Institute IPEN-CNEN/SP, Cidade Universitária "Armando de Salles Oliveira", 2242 Prof. Lineu Prestes Avenue, São Paulo, SP 05508-900, Brazil

ARTICLE INFO

Keywords:
Yttria-stabilized zirconia polycrystal
Hydrothermal ageing
Mechanical properties
Transformed zone
Phase transformation kinetics

ABSTRACT

This study aimed to validate the Optical coherence tomography (OCT) for the analysis of the transformed zone of two dental zirconia-based materials after hydrothermal ageing and correlate the values with biaxial flexural strength. Kinetics of tetragonal to monoclinic phase transformation (t→m) was calculated. X-ray diffraction (XRD) results showed a sigmoidal transformation rate over time due to the limited X-ray maximum penetration depth. Scanning electron microscope (SEM) and OCT showed a linear relationship between the thickness of the transformed layer and the ageing time. The apparent activation energy was 104.5 kJ/mol and 106.7 kJ/mol (SEM) and 106 kJ/mol and 99.4 kJ/mol (OCT) for the infrastructure and monolithic dental zirconia, respectively. Mechanical strength decreased after 150 h. of ageing at 150 °C for both materials showing a correlation with the depth of the transformed zone observed by OCT. Therefore, both monoclinic phase percentage and the depth of the transformed layer are critical concerning zirconia mechanical properties upon hydrothermal ageing. OCT is a non-destructive, fast, innovative, and accurate method for the analysis of zirconia's t→m phase transformation depth kinetics after hydrothermal ageing.

1. Introduction

The increased esthetic demand in fixed prosthodontics has led to the use of all-ceramic crowns with emphasis on yttria-partially stabilized zirconia (Y-PSZ) [1,2]. This type of material combines a whitish color with superior mechanical properties and is used for infrastructures (substructure or core material) or monolithic restoration [3].

The high fracture strength of Y-PSZ is a consequence of its toughening mechanism [4,5], resultant from the tetragonal to monoclinic transformation (t→m), which may halt a crack from propagating due to local granular volumetric expansion in the range of 3-5% [6]. However, in a humid environment at body temperature, Y-PSZ presents an accelerated t→m phase transformation denominated "low temperature degradation" (LTD) [7–9], uncontrolled phase transformation may lead to grain pull-out and microcracks [7]. This phenomenon can decrease the Young's modulus, hardness and biaxial flexure strength and eventually lead to the catastrophic failure of the material [7,10–12]. However, the literature is conflicting concerning the increase/decrease of the

Abbreviations: t→m, tetragonal to monoclinic phase transformation; SEM, Scanning electron microscoe; XRD, X-ray diffraction; OCT, Optical coherence tomography.

* Corresponding author: Nuclear and Energy Research Institute IPEN-CNEN/SP, Cidade Universitária "Armando de Salles Oliveira", 2242 Prof. Lineu Prestes Avenue, São Paulo, SP, 05508-900, Brazil.
E-mail address: aaratafo@uwo.ca (A. Arata Found).

[1] This paper is dedicated to the memory of Prof. Valter Ussui, who passed away on January 21st, 2021.

https://doi.org/10.1016/j.mtla.2023.101825
Received 18 May 2020; Accepted 18 June 2023
Available online 19 June 2023

Y-TZP mechanical strength after short periods of LTD [13–16]. The correlation between LTD and mechanical resistance of Y-TZP is still unclear.

Chevalier et al. (1999) [7] calculated the activation energy for the t→m phase transformation of one biomedical yttria-stabilized tetragonal zirconia (Y-TZP), and observed that 1 hour of hydrothermal ageing at 134°C was theoretically related to 3-4 years of *in vivo* ageing at 37°C [7, 9]. However, the authors suggested that microstructure, amount of yttria, residual stress, finishing procedures, grain size and other factors may affect the LTD behavior of different Y-PSZ materials [7,14,17].

X-Ray Diffraction (XRD) results indicate that Y-TZP t→m transformation follows a sigmoidal behavior upon ageing, where the transformed monoclinic phase reaches a saturation point, stabilizing the percentage of final monoclinic phase as a function of the ageing time [7]. This sigmoidal behavior of Y-TZP ageing seems to be related to the XRD technique [18], which is limited by the X-ray maximum penetration depth. Studies have suggested that LTD t→m transformation follows a linear behavior [18–20]. Scanning Electron Microscopy (SEM) coupled with Focused Ion Beam (FIB) was reported as one of the techniques for Y-TZP microstructure analysis upon ageing [18]. Nevertheless, the sample preparation procedures, such as cutting and polishing, may have an effect on the final Y-TZP microstructure. Therefore, a non-destructive technique that requires no sample preparation would be more reliable for Y-TZP t→m analysis.

Optical Coherence Tomography (OCT) is a non-destructive and non-contact image technique based on light backscattered from a surface [21]. OCT produces cross-sectional tomographic high-resolution images (usually in the range of a few micrometers) with good penetration depth (in the order of a few millimeters). OCT systems are compact, and the wavelength range of operation is usually on the near infrared range (750 – 1400 nm), which means it employs non-ionizing radiation. OCT is usually mounted on a Michelson interferometer, in which a broadband light source is split by a Beam Splitter (BS) into two optical paths, one directed to a mirror (reference arm) and the second to the sample (sample arm). The reflected and backscattered beams are recombined and directed to a detector, which produces an interferometric signal. The key of OCT analysis is that the intensity of the detected interferometric signal (light backscattered from different depths of the sample) will induce a predictable oscillation on the OCT signal, and each depth can be recovered by an inverse Fast Fourier Transform (FFT) [22]. With the information of each depth, a tomographic profile (directly underneath the point illuminated by the beam), is obtained. By scanning the beam through different adjacent locations, 2D images (or 3D volumes) of tomographic structures are generated [23–25]. Thus, OCT systems can produce high-resolution tomographic images in real time (or even entire volumes, using modern systems), without any need of additional sample preparation, enabling a high volume of analysis in a short time.

The aim of this study was to validate the OCT method for the t→m analysis of different zirconia materials upon hydrothermal ageing. The kinetics of t→m transformation was also calculated. Specifically, the objectives were: a) To compare the activation energy of t→m transformation calculated by XRD, SEM, and OCT; b) To evaluate the correlation between the percentage of monoclinic phase, depth of the transformed zone as a function of hydrothermal ageing time and biaxial flexural strength. The study null-hypotheses were: the activation energy calculated for both zirconia-based materials would not be affected by the method employed (XRD, SEM or OCT); the biaxial flexural strength of both materials would not be affected by different ageing times at 150°C.

2. Materials and methods

2.1. Experimental materials

Pre-sintered blocks of 3 mol% Y-TZP for infrastructure (VITA In-Ceram YZ, VITA Zahnfabrik, Germany) and for monolithic (LAVA Plus, 3M-ESPE, USA) restorations were machined and they were sectioned to the following dimensions: Ø 15 mm x 2 mm thickness. The samples were ground and polished using 400-, 600-, 1200-, 2400- and 3000- grit silicon carbide paper (Norton Saint-Gobain, Brazil) under water cooling and were ultrasonically cleaned in isopropyl alcohol for 15 min. Specimens were sintered following manufacturers' instructions in an electrical box furnace (Lindberg/Blue M, Asheville, NC, USA). The density of the as-sintered ceramics was determined by the Archimedes Method. One sample of each material was polished with ceramographic cloth and 15, 9, 6, 3 and 1 μm diamond suspensions (Mecapol P320, Presi, Grenoble, France), respectively, for post-sintering microstructure morphology analysis. The specimens were subjected to thermal etching at 1400°C for 1 hour and were analyzed by a field scanning electron microscopy (FEG-SEM, JSM-6701F, Jeol, Japan) and X-ray energy-dispersive fluorescence spectroscopy (RX-3000, Rigaku, Japan).

2.2. Accelerated ageing

The specimens (n=4 per material) were aged in a hydrothermal pressurized reactor (4566 Minireactor, Parr Instrument, USA) as a function of temperature (100°C, 120°C, 130°C and 150°C). A prior pilot study was performed with different Y-TZP materials in order to establish the different ageing times (h) presented in this study according to the t→m phase transformation kinetic curve. Different methods were used to determine the ageing kinetics as a function of t→m increase mode: a) Sigmoidal behavior: XRD; b) Linear behavior: XRD, SEM and OCT.

2.3. Sigmoidal model - XRD

XRD analysis (X'pert Powder, PANalytical, Netherlands), Cu-Kα (λ = 1.54060 Å), 45 kV, 40 mA was used to calculate t→m transformation rate. Scans were performed from 2θ, 20^{o} to 80^{0}, step size of 0.02^{o}; 10 s per step. The maximum X-ray penetration depth was calculated using the density of the tetragonal, monoclinic and cubic phases Eqs. 1 and (2) [26].

$$K_x = \left(1 - e^{\frac{-2\mu x}{\sin\theta}}\right) \tag{1}$$

$$x = -\frac{\ln(1 - K_x)\sin\theta}{2\mu} \tag{2}$$

Where:

x – Depth of x-ray penetration (cm)
K_x – Total diffracted intensity (95%)
μ – Linear absorption coefficient
θ – Incident and refracted angle

The mass absorption coefficient (μ_m) was obtained from the Eq. 3 [27].

$$\mu_m = \frac{N_A}{MW}\sum_i x_i \sigma_{ai} \tag{3}$$

Where:

N_A - Avogadro's number,
MW - molecular weight
x_i - number of *i*-type atoms per molecule
σ_{ai} - atomic photo absorption cross section of the *i*-type atom.

The linear absorption coefficient (μ_l) was calculated using the weighted average of the mass absorption coefficient (μ_m) multiplied by the density of each phase. The μ_m values used in this present study for the tetragonal, monoclinic and cubic phase were 647.88, 616.01, and 646.81, respectively.

The percentage of tetragonal, monoclinic and cubic phase was calculated through the Rietveld refinement using the program *General Structure Analysis System* (GSAS) [28]. The crystal structure data (atom coordinates, thermal parameters and unit cell parameters) were obtained from the Inorganic Crystal Structure Data Base – ICSD. The computation adjustments were the scale factors, unit cell parameter, pattern background polynomial parameter, 2θ-scale offset, peak profile functions (pseudo-Voigt with asymmetry), and texture.

The Mehl-Avrami-Johnson equation modified by Kolmogorov (Johnson-Mehl-Avrami-Kolmogorov – JMAK) was used based on the finding of Chevalier et al. (1999) [7] to calculate the correlation between ageing time (t) and monoclinic phase content (V_m), assuming values lower than 100% of monoclinic saturation for all the temperatures studied (Eq. 4):

$$V_m = V_{m0} + \left(V_{mf} - V_{m0}\right)\{1 - \exp\{-\ [(bt)^n]\}\} \tag{4}$$

Where:

Vm_0	Amount of initial monoclinic phase
V_{mf}	Amount of monoclinic phase saturation
b	Parameter dependent of the rate of nucleation and monoclinic growth speed
n	Avrami exponent – type of spatial grain growth

2.4. Linear Model

2.4.1. XRD analysis

For XRD analysis, the infrastructure Y-TZP was aged at 130°C for 20, 30, 40 and 84 h.. The relative vertical t→m depth was analyzed by XRD with fixed incidence angles (2°, 3°, 5°, 7° and 12°) [18], and the X-ray penetration depth was calculated according to Eqs. 5 and 6 [26].

$$K_x = 1 - e^{-\mu x\left(\frac{1}{\sin\ \gamma} + \frac{1}{\sin\ \beta}\right)} \tag{5}$$

$$x = -\frac{\ln(1 - K_x)}{\mu\left(\frac{1}{\sin\gamma} + \frac{1}{\sin\beta}\right)} \tag{6}$$

Where:

X – Depth of X-ray penetration (cm)
K_x – Total diffracted Intensity (95%)
μ – Linear absorption coefficient
ϒ – Incidence angle
β – Diffraction angle

2.4.2. SEM analysis

One sample of control and aged groups (120°C, 130°C and 150°C in different times) (N=14 insfrastructure, N=10 monolithic), were perpendicularly cross-sectioned and sequentially polished with 15, 9, 6, 3 and 1 μm diamond suspensions deposited over a ceramographic cloth (Mecapol P320, Presi, Grenoble, France). Back-scattered SEM (TM 3000, Hitachi) was used to calculate the depth of t→m transformed zone with an image analysis software (Image J, Public domain, USA).

2.4.3. OCT analysis

Four samples of each group (control, 120°C, 130°C and 150°C in different ageing times) (N=36 infrastructure, N=36 monolithic), were analyzed under optical coherence tomography (OCP930SR, Thorlabs Inc.) as follows: λ= 930 nm, spectral band (FWHM) of 100 nm, nominal resolution of 6 μm (lateral and axial) in air, declared digital resolution 3.09 μm (axial). The refractive index of each material was calculated and used to correct the resulting images, as the optical path of the OCT beam inside the sample is affected by refraction. Five areas of 3 mm (lateral) were obtained in each sample to calculate t→m transformed zone depth using Image J. The speed of the transformation zone (μm/h) was determined plotting the t→m phase transformation depth versus ageing time for the SEM analysis and for the OCT analysis through the angular coefficient of the linear adjustment in all studied temperatures.

2.5. Activation energy analysis

The angular coefficient data ln(b) and ln(s), obtained for the sigmoidal (XRD) and linear models (SEM and OCT) for each studied temperature (1000/T) (K), were used to calculate the t→m energy of activation following Arrhenius model (Eq. 7) [7]. The activation energy (Ea) is defined as the energy barrier that the tetragonal phase needs to overcome to transform to monoclinic phase [29].

$$b = b_0 \exp\left(\frac{-Ea}{RT}\right) \tag{7}$$

Where:

b	Speed constant
b_0	Pre exponential factor
Ea	Activation energy
R	Gas constant
T	Temperature (K)

The XRD data of t→m rate and the SEM and OCT data of the speed of the transformed zone increase (μm/h) were extrapolated to body temperature (37°C). The comparison of the results between SEM and OCT were used to validate OCT as a method of analysis for the calculation of depth and speed of t→m transformed zone.

2.6. Biaxial flexural strength

The as-sintered specimens (n=10 infrastructure/n=8 monolithic), 12 mm of diameter and height of 1.2 to 2 mm, were aged at 0, 5, 25, 70, and 140 h. (150°C/3.01 bar) and submitted to biaxial flexural strength test, according to the ISO 6872, 2008 [30]. The disc-shaped specimens were positioned on three support balls (ø= 1.88 mm), positioned 10 mm apart of each other. An increasing load was applied (1 mm/min cross-head speed, water, room temperature) in a universal testing machine (Instron 8501, USA) until fracture. Biaxial flexural strength (MPa) was calculated using Eqs. 8, 9, and 10.

$$\boldsymbol{\sigma} = -0.2397\frac{\boldsymbol{P}(\boldsymbol{X} - \boldsymbol{Y})}{\boldsymbol{b}^2} \tag{8}$$

Where:

σ = maximum tensile stress (MPa)
P = total load causing fracture (N)
b = specimen thickness at the origin of the fracture (mm)

$$X = (1+\nu)\ln\left(\frac{r_2}{r_3}\right)^2 + \left[\left(\frac{1-\nu}{2}\right)\left(\frac{r_2}{r_3}\right)^2\right] \tag{9}$$

$$Y = (1+\nu)\left[1 + \ln\left(\frac{r_1}{r_3}\right)^2\right] + (1-\nu)\left(\frac{r_1}{r_3}\right)^2 \tag{10}$$

Where:

ν = Poisson's ratio (0.31)
r1 = radius of the support circle (mm)
r2 = radius of the loaded area (mm)
r3 = radius of the specimen (mm)

Table 1
Phase fraction (Rietveld refinement), theoretical density, apparent density, grain size, and biaxial strength of the infrastructure and monolithic Y-TZP sintered at 1530°C for 2 h and 1450°C for 2 h, respectively.

	Infrastructure	Monolithic
Tetragonal phase content (wt%)	81.21±4.1	77.41 ±4.6
Monoclinic phase content (wt%)	-	-
Cubic phase content (wt%)	18.79±4.1	22.59 ±4.2
$\rho_{theoretical}$ (g cm^{-3})	6.1	6.1
$\rho_{apparent}$ (g cm^{-3})	6.01	6.0
$\rho_{relative}$ (%)	98.5±0.1	98.72±0.1
Grain size (nm)	705±0.3	778±0.8
Biaxial strength (MPa)	1053±76.8	1059±135.8

To establish a correlation between t→m transformation growth and mechanical properties, data of OCT (n=10 infrastructure/n=8 monolithic) and biaxial flexural strength test were analyzed as a function of ageing time: 0, 5, 25, 70 and 140 h. (150°C/3.01 bar) [30].

2.7. Data analysis

Data was subjected to descriptive and inferential statistical analysis (IBM SPSS Statisticsversion 21.0, 2012, IBM Armonk, New York, USA). Flexural strength data (MPa) was analyzed by one-way Analysis of Variance (ANOVA) and Tukey's test for the infrastructure groups and Welch's ANOVA and Dunnett T3 for the monolithic groups (α= 0.05). Normal distribution of data and homogeneity of variance were checked using the Shapiro-Wilk and Levene tests, respectively (α= 0.05). Pearson's chi-squared test was used at a significance level of $p<0.05$ to correlate the depth of t→m transformed zone and flexural strength for both materials.

3. Results

3.1 Zirconia characterization

Both as-sintered materials showed similar apparent densities, grain size and biaxial strength (Table 1). Figs 1a and 1b show similarities at the insfrastructure and monolithic Y-TZP microstructures, respectively. According to the manufacturer, both ceramics present 3mol% of Y-TZP and < 0.1 wt% of Al_2O_3.

3.2. Analysis of Sigmoidal Model by XRD

The results of the kinetics of phase transformation for both materials as a function of the amount of monoclinic phase calculated by XRD results are presented in Table 2 and Fig. 2a-b. Amongst the temperatures analyzed in this study, the higher the temperature, the faster the t→m transformation rate and the monoclinic phase stabilization occurred around 60-67% for both materials. Table 2 also shows a constant speed (percentage of monoclinic phase transformation), as a result of JMAK equation for each studied temperature. The activation energy was 93.16 kJ/mol and 107.58 kJ/mol for the infrastructure and monolithic Y-TZP, respectively (Fig. 2c-d).

The activation energy values allowed the prediction of the t→m at 37°C for both ceramics. Theoretically, one year of hydrothermal ageing at 37°C will result in approximately 12.3 (±5.7) % and 4.30 (±1.3) % of monoclinic phase for the infrastructure and monolithic zirconia, respectively. Based on the extrapolated data, in humid environment at 37°C, infrastructure zirconia will present 33.2 (±11.7)% of monoclinic phase after 5 years and 45.6 (±12.1) % of monoclinic phase after 10 years; and monolithic zirconia will present 15.3 (±4.4) % of monoclinic phase after 5 years, and 24.9 (±6.3) % of monoclinic phase after 10 years.

Fig. 3a shows the maximum X-ray penetration depth according to Eqs. (1) and (2). Higher peaks of the tetragonal and monoclinic phases are located in the range of 28-31° (2θ analysis). Therefore, the angle 30° (2θ) was selected to evaluate the maximum X-ray penetration depth; for a sample containing 100% of monoclinic phase, the maximum X-ray penetration is 6.3 μm. The impact of the 6.3 μm XRD penetration on the percentage of monoclinic phase for infrastructure Y-TZP aged at 130°C is presented in a schematic drawing (Fig. 3b). After 25 h. of hydrothermal ageing, the XRD penetrated deeper than the transformed layer (2.6 μm observed by SEM). Then, the percentage of monoclinic phase was the weighted average between the transformed and untransformed layer, resulting in a lower amount of monoclinic phase (observed in the

Table 2
Parameters of the JMAK equation obtained by the experimental data fitting, showing the t→m kinetics at different temperatures (mean±SD).

		100°C	120°C	130°C	150°C
Infrastructure	n	0.82 (0.19)	0.77 (0.10)	0.63 (0.03)	0.83 (0.09)
	b	0.006 (0.0)	0.02 (0.00)	0.07 (0.003)	0.21 (0.01)
	r^2	0.96	0.96	0.99	0.99
Monolithic	n	0.67 (0.16)	0.99 (0.21)	0.97 (0.25)	0.59 (0.15)
	b	0.005 (0.0)	0.02 (0.0)	0.05 (0.10)	0.36 (0.06)
	r^2	0.97	0.98	0.95	0.99

b - Parameter dependent of the rate of nucleation and monoclinic growth speed parameter.
n- Avrami exponent – type of spatial grain growth (Eq. 4).
r^2- chi-square adjustment.

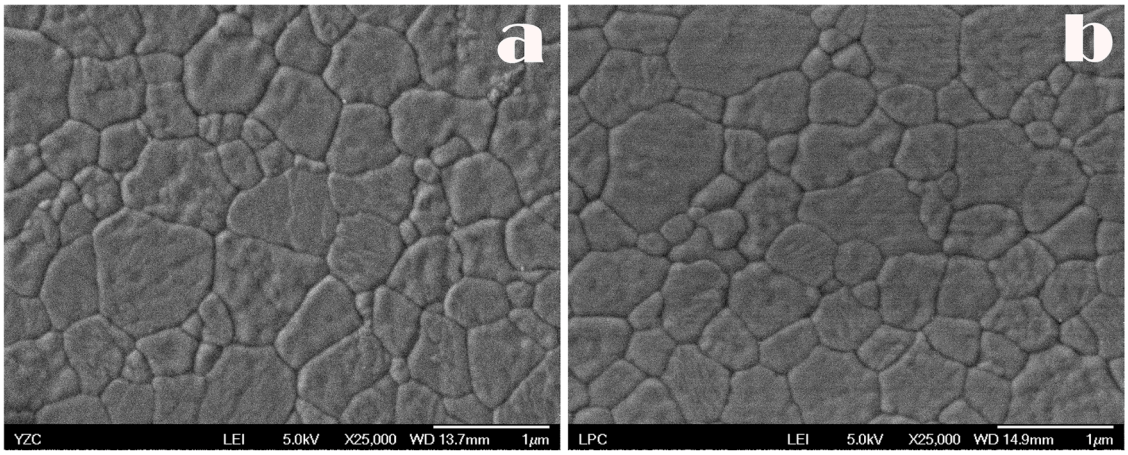

Fig. 1. FEG-SEM micrographs of the cross section showing the microstructure of the infrastructure (a) and monolithic (b) ceramics sintered at 1530°C for 2 h and 1450°C for 2 h, respectively.

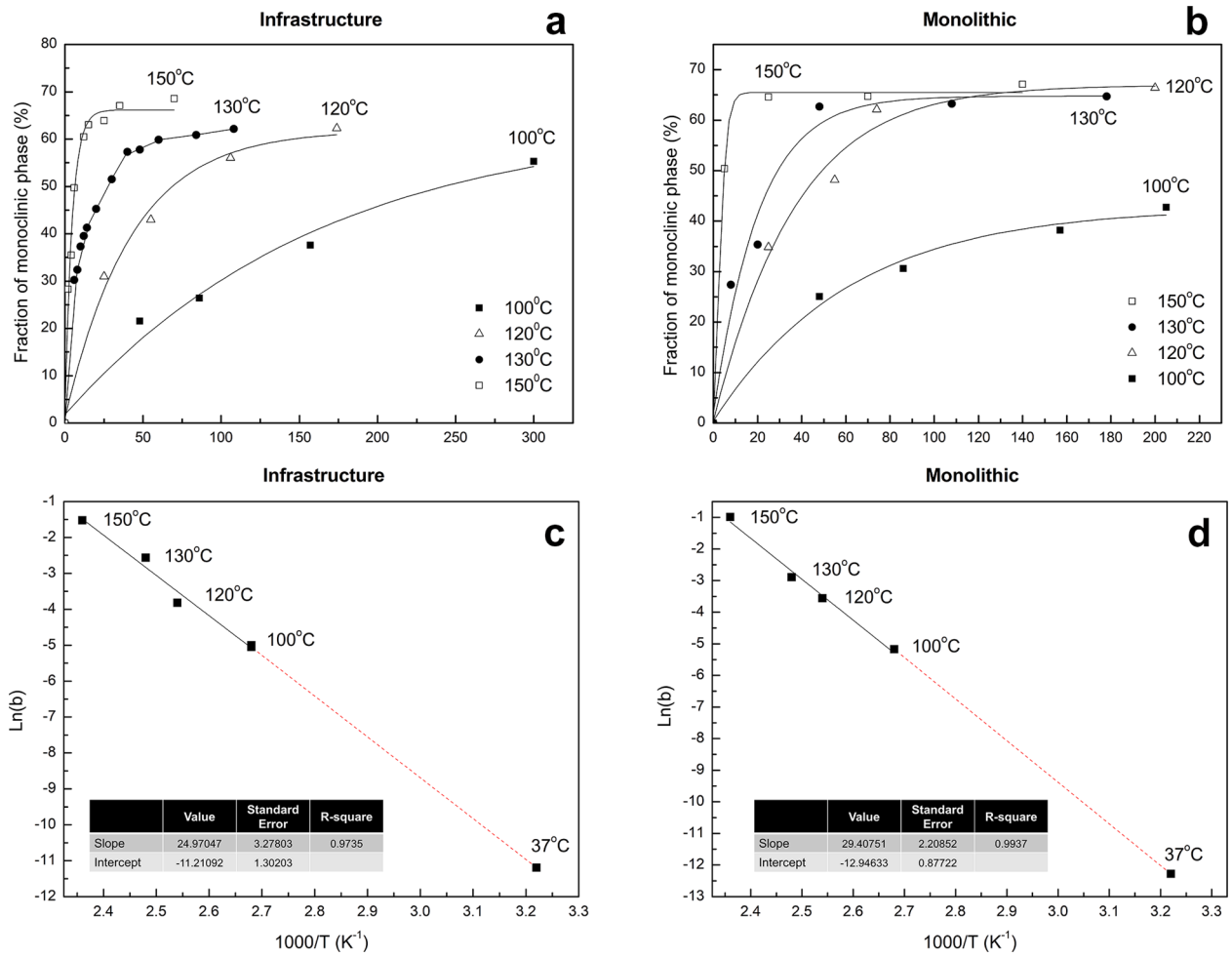

Fig. 2. Kinetic curves of phase transformation (a, b) of the infrastructure and monolithic ceramics calculated through Johnson-Mehl-Avrami-Kolmogorow – JMAK equation and respectively Arrhenius plot of ln(S) vs. 1000/T (c, d) allowing the determination of the apparent activation energy of the ageing process and extrapolation of ageing kinetics to a body temperature of 37°C.

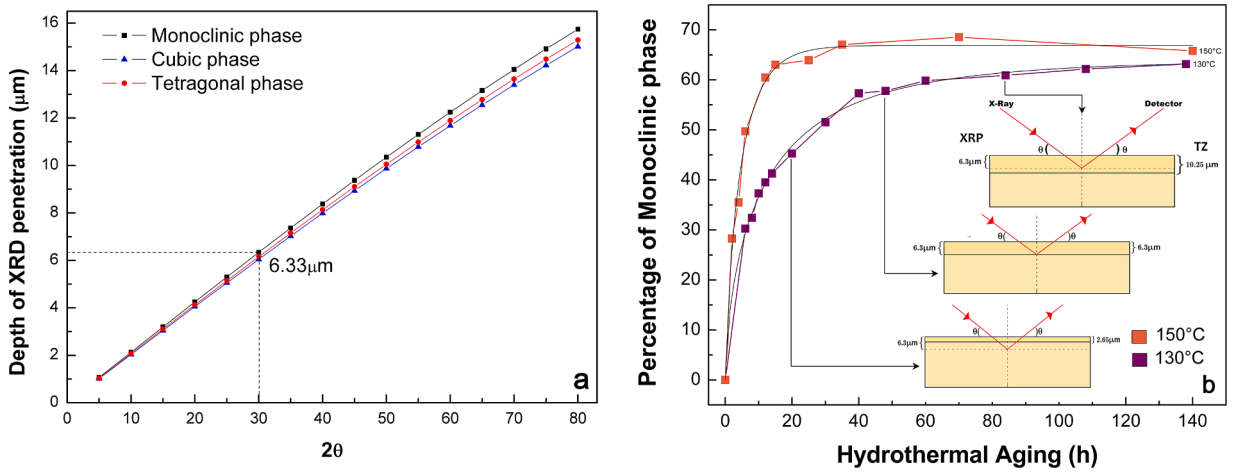

Fig. 3. XRD analysis for Y-TZP infrastructure ceramic: a) Depth of X-ray penetration (μm) where values were calculated for the Y-TZP tetragonal, cubic and monoclinic phase with 30° (2θ) and CuKα irradiation; b) Sigmoidal effect due to the limitation of the X-ray penetration in relation to the t→m transformed zone.

kinetic curve of t→m). When the depth of the transformed zone is equal to the XRD maximum penetration, the first saturation point of the monoclinic phase is observed on the curve. After 48 h. of hydrothermal ageing, the transformed zone (10.2 μm) is deeper than the XRD penetration (6.3 μm) and, therefore the analysis shows a stabilization of the monoclinic phase percentage, known as "saturation point". Despite the increasing depth of the transformed zone over time, the amount of monoclinic phase detected by XRD stabilizes (~65%). These results were a critical evidence that the sigmoidal behavior of zirconia materials after LTD were a result of the limited depth of penetration of the XRD.

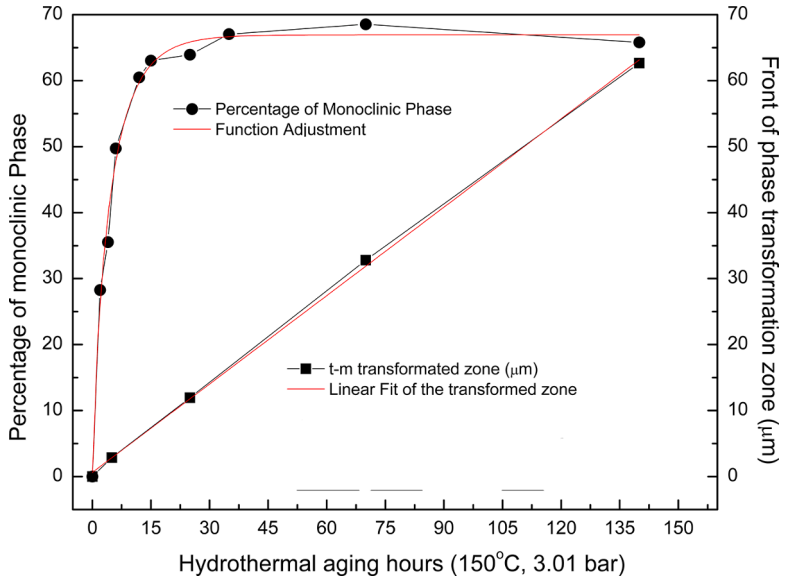

Fig. 4. Comparison of the XRD and SEM data of the t→m phase transformation: the Avrami curve (●) shows that the monoclinic phase was stabilized after 15 ageing h. and the linear curve (■) demonstrates that the front of phase transformation zone advances linearly into the bulk.

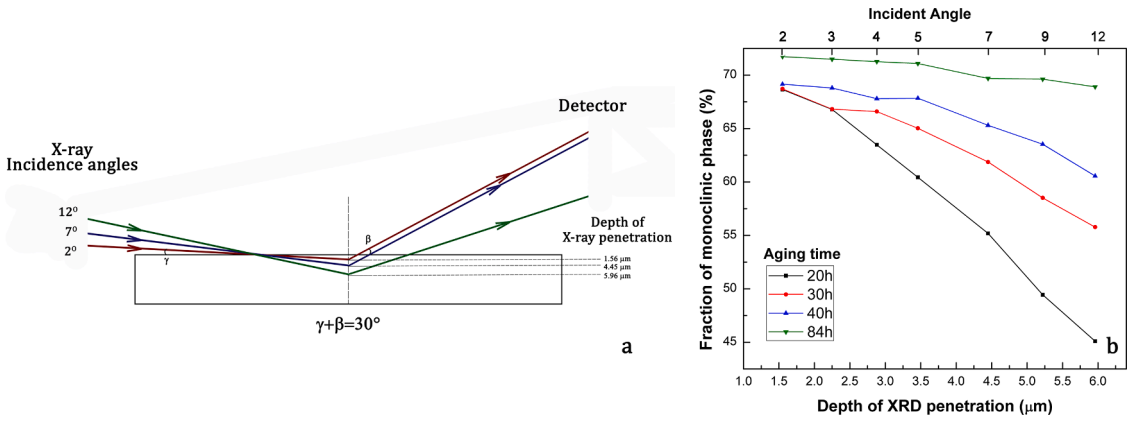

Fig. 5. XRD analysis for Y-TZP infrastructure ceramic: a) Influence of the incidence angle at the X-ray penetration depth; b) Fraction of monoclinic phase of the infrastructure according to the X-ray incidence angle and ageing time at 130°C.

Fig. 4 shows the comparison of the XRD sigmoidal effect and the SEM linear results.

3.3. Linear behavior

The depth of XRD penetration varied between 1.55 μm and 5.96 μm, when varying the incidence angle from 2° to 12° (Fig. 5a schematic drawing), with lower angles presenting lower analytical depth. The XRD analysis at 2° (maximum X-ray penetration of ~1.55 μm) showed 65-68% of monoclinic phase for insfrastructure Y-TZP aged during 20 h. at 130°C (transformed zone ~2.6 μm measured by SEM) (Fig. 5b). This result is reached after 40 h. of hydrothermal ageing, from 20° to 80° at the 2θ analysis (Fig. 3b). Moreover, for specimens aged for 20 h. measured with lower incidence angles, and consequently lower penetration depth, XRD indicated higher amounts of monoclinic phase. Nevertheless, higher incidence angles (higher X-ray penetration) showed lower amounts of monoclinic phase. This effect is related to the average between the amount of transformed and untransformed layer, which is characteristic of the XRD analysis. The same results were observed at 30h and 40h (transformed zone = 3.70 μm and 5.21 μm, respectively). However, longer times, such as 84 h. of hydrothermal ageing (transformed zone =10.25 μm), decreased the variation of the monoclinic phase concentration, resulting in similar amount of transformed phase regardless of the X-ray incidence angle (Fig. 5b). The distribution of monoclinic phase was homogenous through the whole transformed zone, and the transformed layer started at a fixed amount of monoclinic phase at 2° that was the same throughout the layer (from 4-12°) in function of ageing time (Fig. 5b).

SEM of cross-sectioned control and hydrothermally aged (120°C, 130°C and 150°C) specimens indicated a linear growth of the transformed zone from the surface to the bulk of both materials (Fig. 6). At a larger magnification, pores and grain pullout associated with a "microcracked" zone were observed (Figs. 7 and 8). SEM showed that the growth of the transformed zone was still not stable after 15 h. of ageing.

When the transformed zone depth of infrastructure and monolithic Y-TZP were analyzed by OCT (Fig. 9) and SEM (Fig. 6), no transformation was observed for 5h at 150°C. After 25 h and 35 h of ageing, an opaque layer, which indicates t→m transformation, was detected and showed to increase over time. The layer was more evident at 70, 140 and 280 h., indicating the linear growth of the transformed zone. The same behavior was observed when the same materials were aged at 130°C and 120°C (Figs 6 and 9).

To assess the transformed layer depth by OCT, the measurements

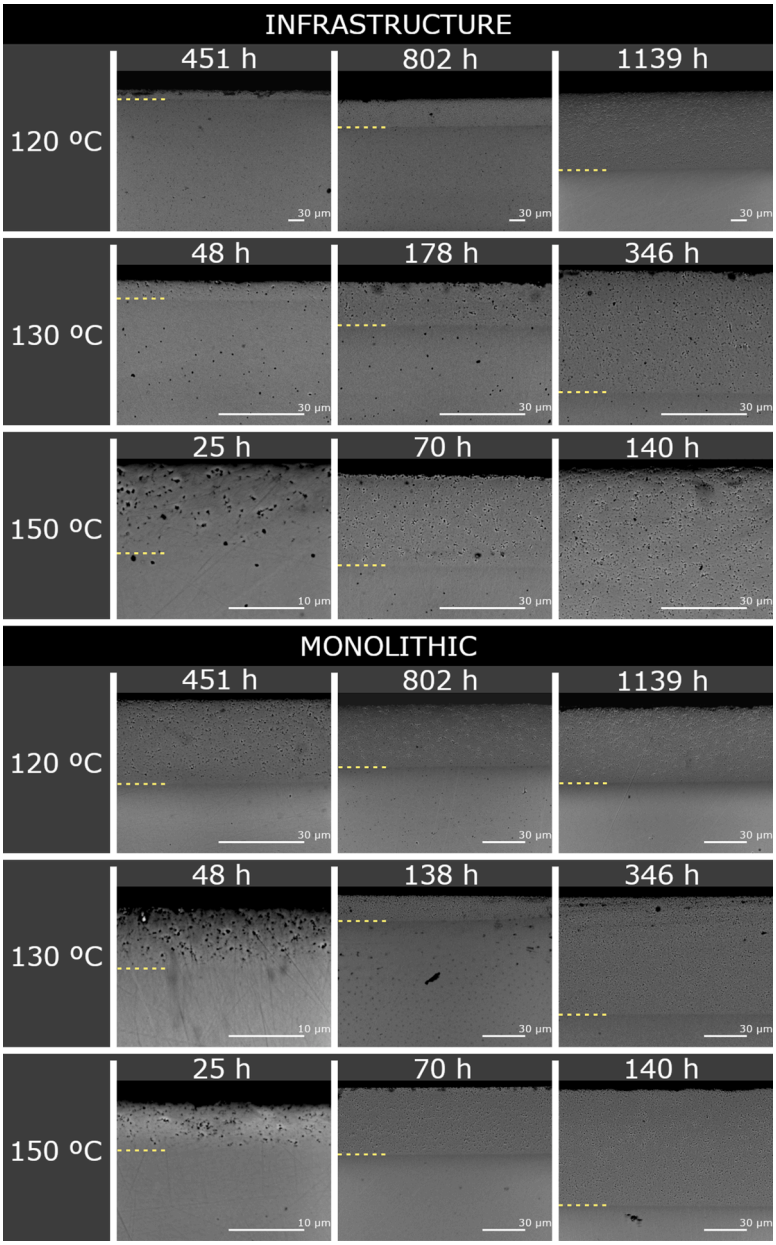

Fig. 6. SEM comparing the depth of the transformed zone of the infrastructure and monolithic group after hydrothermal ageing at 120°C, 130°C and 150°C at different ageing times.

were corrected by the refractive index of the materials. The ratio between the physical distance of the transformed layer (measured by SEM) and the optical distance (observed depth in the OCT), yields the refractive index of interest, which resulted in 2.09 (± 0.39) and 2.17 (± 0.39) for the infrastructure and monolithic zirconia, respectively. OCT values were, henceforth, divided by the refractive index, and the real value of the transformed zone depth was calculated (μm) for each sample. The transformed zone depth values obtained by SEM (cross-sectional) and OCT for both materials are presented in Fig. 10 (a and b). Both techniques indicated similar transformation kinetics, with the depth of the transformed zone increasing as a function of ageing time and temperature regardless of the material. Transformation depth values were used for calculating the speed rate of the t→m growth for each temperature (Fig. 10a-b). Based on SEM, Ea were 104.5 kJ/mol and 106.7 kJ/mol, while OCT indicated 106 kJ/mol and 99.4 kJ/mol for infrastructure and monolithic Y-TZP (Fig. 10c and 10d), respectively. When the results were extrapolated to body temperature (37°C), the ageing rate was 0.07 (±0.016) μm/year and 0.17 (±0.05) μm/year based on SEM data and 0.08 (±0.04) μm/year (OCT data) for both ceramics. Table 3 shows a summary of the transformation kinetics based on SEM and OCT data.

3.4. *Biaxial flexural strength after hydrothermal ageing*

For the infrastructure zirconia, one-way ANOVA assumptions of homoscedasticity indicated that the residues were normally distributed (Shapiro-Wilk>0.05) and presented homogeneity of variance (Levene=0.3). ANOVA results indicated that infrastructure Y-TZP flexural strength was significantly affected by hydrothermal ageing time (p=0.001) (Fig. 11a and Table 4). Tukey test (Table 5) results showed that samples aged at 140 h. at 150 °C (849±56 MPa)^{c} presented the lowest values of flexural strength.

Fig. 11b shows the flexural strength values of the monolithic zirconia, which were also normally distributed (Shapiro-Wilk: p≥0.62);

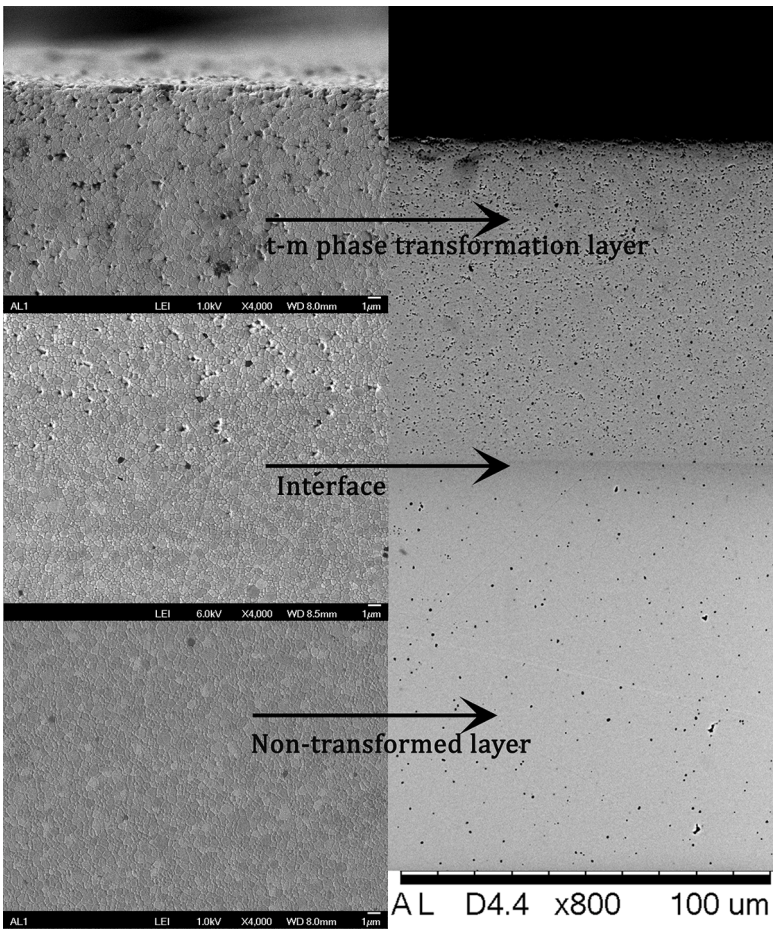

Fig. 7. SEM and FEG-SEM micrographs of an infrastructure cross-sectioned sample aged for 140 h at 150°C, comparing the transformed layer, the interface between the layers and the non-transformed layer.

however, they did not present homogeneity of variance (Levene: p=0.04). Therefore, one-way ANOVA was performed with a Welch correction (p= 0.011) that showed a significant effect of ageing time (Table 4). Table 5 shows the Dunnett T3 test indicating that samples aged for 140 h. presented the lowest flexural strength (883±53 MPa)^{c}, but the results were similar to samples aged for 5 h and 70 h.. The estimated time at body temperature (37°C) hydrothermal ageing to achieve the depth of the transformed zone observed by SEM and OCT at 150°C is shown in Table 5.

The Pearson correlation of transformed zone depth (OCT) and biaxial flexural strength showed a significant negative correlation (α=0.00* and α=0.01*) for both materials (r= -0.78 and r= -0.66), infrastructure and monolithic, respectively indicating that the higher the depth of the transformed zone, the lower the flexural strength.

4. Discussion

Y-TZP was initially used as an infrastructure material in single or multi-element fixed dental prosthesis, veneered with a porcelain. However, problems with the veneering material [31,32] and the interface between porcelain and Y-TZP prompted the development of the monolithic translucent Y-TZP [12,33,34]. To increase Y-TZP translucency it is necessary to decrease the light scattering around grain boundaries [35,36]. However, this procedure may decrease the mechanical strength of the ceramic [37]. The addition of dopants that may segregate to the grain boundary, the sintering protocol, and the grain size can also influence the translucency [35,38,39].

Both materials analyzed in the present study presented similar density value and an average of 700-800 nm grain size, which makes the microstructure very similar between the two materials. Despite of the difference in sintering temperature, both ceramics presented high densification (~98%) when compared to the Y-TZP theoretical densification. The monolithic Y-TZP presented lower concentration of alumina in comparison to the infrastructure material to improve the translucency [40].

XRD is the most frequently used technique to evaluate the tetragonal-to-monoclinic Y-TZP phase transformation. It is a non-destructive method suggested by the ISO standard #13356 for crystalline phase identification [41]. However, its accuracy to identify small amounts of monoclinic phase (lower than 2%) is questionable, due to the similarity between the intensity and the noise ratio. Furthermore, XRD is a superficial analysis, limited to the X-ray penetration depth (~5 to 10 μm) depending on the material [9]. Y-TZP transformation kinetics analyzed by XRD has shown a sigmoidal t→m transition as a function of time [7, 42–46]. However, previous studies have shown that the kinetics of phase transformation follows a linear model, where the thickness of the transformed layer increases linearly with time into the bulk of the Y-TZP [18–20]. When one does not take into consideration the depth of analysis, the sigmoidal curve presented by XRD is a consequence of the maximum penetration depth of the X-ray (6.3 μm) [26,47], which leads to an erroneous interpretation of the amount of transformed monoclinic phase. When the transformed layer is greater than the maximum X-ray penetration depth, the degradation cannot be further detected by the XRD technique, indicating a saturation [41]. Fig. 3b shows how the limited XRD penetration depth affects the detection of monoclinic phase. Varying the grazing angle allows the analysis of the depth profile of the amount of monoclinic phase [41,47,48]. Decreasing the analysis depth allowed a signal rate increase at the specimen surface, and a

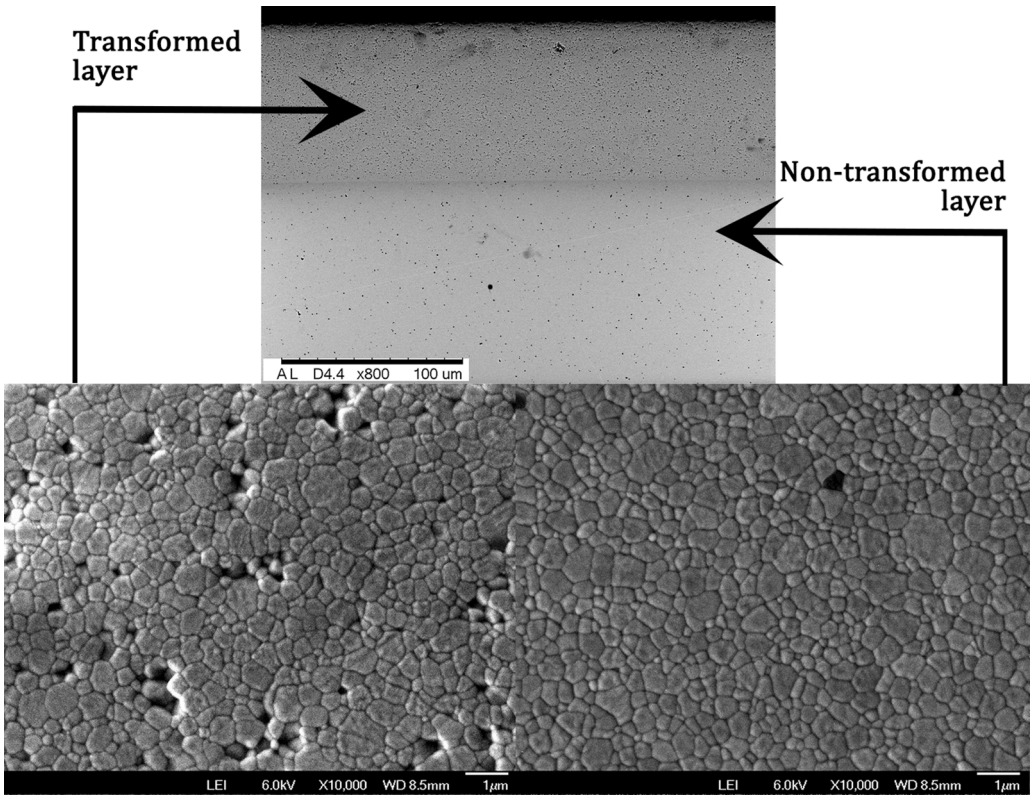

Fig. 8. SEM and FEG-SEM micrographs of an infrastructure cross-sectioned sample aged for 140 h at 150°C comparing the non-transformed layer and transformed layer microstructure, especially the porosity and grains dimensions.

higher apparent amount of monoclinic phase was detected. Within this depth range (2-12º angle, 1.55-5.96 μm penetration depth) XRD results showed that the Y-TZP hydrothermal ageing is a uniform evolution process (Fig. 5b). The determination of the monoclinic phase depth profile can be calculated using the methodology proposed by Gremillard et al. (2010) [47]. Keuper et al. (2013) [18] hydrothermally aged Y-TZP specimens and varied the XRD incidence angle from 1-10°, observing the same t→m phase transformation behavior presented in this study. Despite the possible stabilization of the monoclinic phase at 65% after 15 h. of hydrothermal ageing at 150°C, as shown by XRD, a linear increase of the thickness of the transformed monoclinic phase was observed at different temperatures using SEM (Fig. 4) and OCT technique (Fig. 9). The cross-section of the transformed layer presented grain pullout and pores as a result of the polishing. However, polishing did not affect the surface of the non-transformed zone (Fig. 7 and 8). Chevalier et al. (2011) [19] observed the same linear growth in an aged porous Y-TZP although XRD results indicated a t→m sigmoidal behavior.

Either Garvie and Nicholson equation or the Rietveld refinement method may be used with XRD diffractogram data to calculate the amount of monoclinic phase [28,49,50]. The Garvie and Nicholson modified by Toraya equation is the method frequently used in the literature since it enables direct comparison between many results exposed, however, it is not the most accurate method, especially when the material presents texture. In the present study, the Rietveld refinement technique was used to decrease the error related to the monoclinic phase plane preferential orientation [50], when using the Garvie and Nicholson equation solely. The Rietveld refinement technique integrates the area underneath the peaks from 20-80° (2θ) to calculate the amount of tetragonal, monoclinic and cubic phases. This leads to a more accurate percentage of each phase in comparison to the Garvie and Nicholson equation. However, for the Rietveld refinement it is necessary to increase the time of analysis in order to raise the number of counts per seconds to obtain a more precise diffractogram. For this purpose, a linear detector was used in the present study. Nevertheless, even with this modification, each analysis took 15-20 minutes per specimen.

The Avrami exponent (*n*) for the process that occurs in one dimension is expected to be one, and in the present study, the "n" values were slightly less than 1 for both infrastructure and monolithic Y-TZP. Starink (1997) states that if certain preconditions are met, the Johnson-Mehl-Avrami-Kolmogorov (JMAK) kinetic equation is precisely accurate for nucleation and growth reactions with linear growth [51]. These preconditions include randomly distributed product phases, isotropic growth and a constant equilibrium state. The tetragonal to monoclinic transformation in the ZrO_2 system is an anisotropic martensitic transformation, where the orientation relationship for planes, (100)m / (110) t is established as observed by Arata et al. (2014) for a dental 3Y-TZP ceramic using the Rietveld refinement method [50]. Besides, it is accompanied by volume expansion around 0.05 that causes internal stress, and both indicated the impingement causing deviation of Avrami exponents.

The activation energy for LTD based on SEM data were 104.5 kJ/mol and 106.7 kJ/mol for the infrastructure and monolithic Y-TZP, respectively. The ageing rate was 0.07 (±0.016) μm/year and 0.17 (±0.05) μm/year for the infrastructure and monolithic Y-TZP, respectively. Chevalier et al. (1999) reported an activation energy of 106 kJ/mol for a biomedical 3Y-TZP [7]. For a dental monolithic Y-TZP an activation energy of approximately 98 kJ/mol was calculated [12,52]. The previous studies used the Garvie and Nicholson equation to calculate activation energy, while in the present study the calculation was based on the Rietveld refinement method. The difference among the activation energy could be a result of the methods used to quantify the monoclinic phase and as well be a consequence of the microstructure of the materials analyzed [7].

μ-Raman, SEM, and focused ion bean (FIB) coupled to SEM [9,18,20] are some of the techniques used to show the linear growth of the monoclinic transformed zone [18,20]. However, all of them present

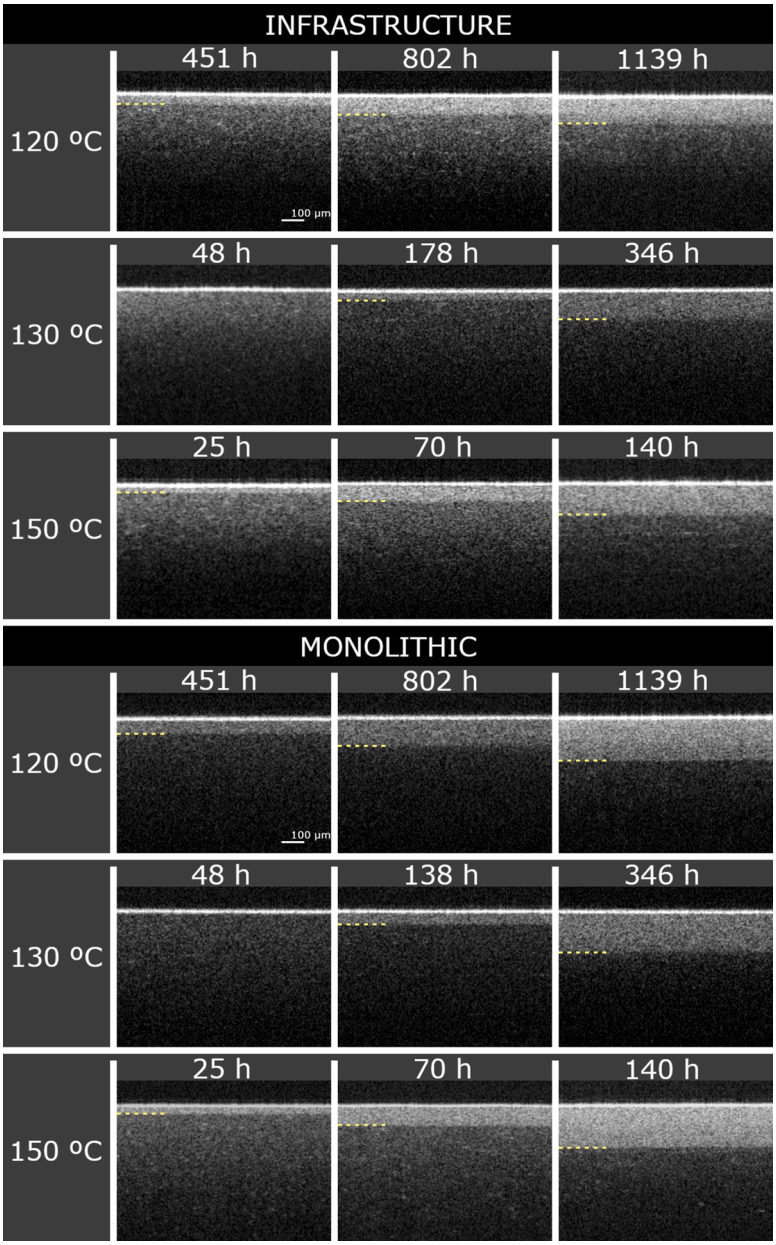

Fig. 9. OCT images of Y-TZP ceramics comparing the depth of the transformed zone of the infrastructure and monolithic group after hydrothermal ageing at 120°C, 130°C and 150°C at different ageing times.

inherent limitations associated with the preparation of Y-TZP specimens, such as cross-sectioning and polishing [53]. Moreover, these are destructive, time-consuming methods.

The OCT is a fast method that may be used for real time analysis and it has been previously used in dentistry for microleakage and bond strength test studies [54,55], but it has not been used for t→m quantification so far. In comparison to SEM, the OCT allowed for faster imaging and analysis, with the only downside of needing a correction for the refractive index (described below). Nevertheless, our OCT images did not reach the same resolution afforded by SEM, which prevented the observation of finer structures. However, newer commercial OCT systems achieve higher resolutions (and better penetration depths) than the system employed in this study. Additionally, the ability to generate 3D tomographic volumes at once enables fast sampling at varying special positions, in contrast to SEM imaging which is limited to a single face of the sample.

OCT showed an “opaque” layer, which is a result of the variation of grain size and spacing in the t→m transformed zone as function of time and ageing temperature. This region with structural changes is detected by the OCT technique since they produce different backscatter intensities, which directly affects the interferometric signal and the corresponding reconstructed sample profile. Therefore, the different grain distribution results in different OCT images. Since OCT is an optical-based technique, it is subject to distortions caused by media with different refractive indexes as it alters the optical path of the beam inside the sample. Therefore, structures on a sample with higher refractive index (RI) appear longer (extended in depth) than the ones on a sample with lower RI. Thus, the determination of RI for the sample under analysis is mandatory to correct the measurements. To obtain the RI for a sample, one only needs to calculate the ratio between the optical path (the one distorted by the RI) and the physical path (the correct measurement) for a known object. Due to the limitations of the OCT equipment used in this study, the refractive index (RI’s) were calculated in conjunction with the SEM data. However, if an OCT image can cover

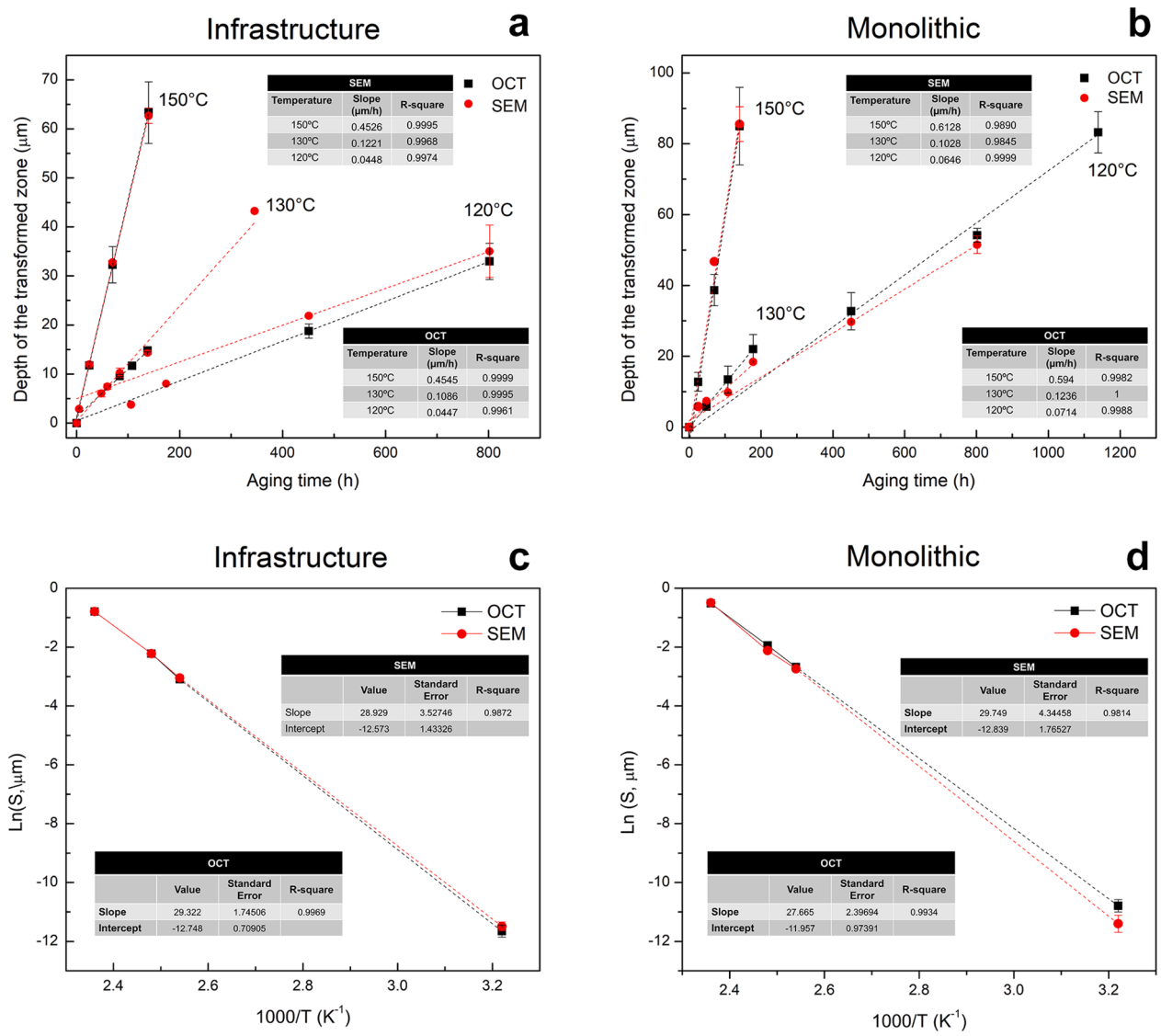

Fig. 10. Comparison of the SEM and OCT results of depth of phase transformation vs hydrothermal ageing time, at different temperatures of infrastructure and monolithic Y-TZP. The slope is the speed of phase transformation (μm/h). The Arrhenius plots of ln(S) vs. 1000/T allow the determination of the apparent activation energy of the ageing process and the extrapolation of ageing kinetics to a body temperature of 37°C.

Table 3
Comparison of XRD, SEM and OCT data for the infrastructure and monolithic ceramic.

	Infrastructure			Monolithic		
	XRD	SEM	OCT	XRD	SEM	OCT
Stabilization of the t→m phase transformation	~65-70	-	-	~65-67	-	-
Apparent Activation Energy (kJ/mol)	93.16	104.5	106	107.58	106.7	99.4
Hydrothermal ageing at 37°C*	12.3 (±5.7)	-	–	4.3(±1.3)	–	–
Ageing rate at 37°C**	-	0.07 (±0.01)	0.08 (±0.04)	-	0.17 (±0.05)	0.08 (±0.04)

* percentage of monoclinic phase (% in one year).
** depth of the transformed zone (μm/year).

the complete sample (the whole depth is included in the image, from top to bottom) and its dimensions are known (i.e., by measuring with a caliper), no further data is required for RI determination – this method is, in fact, preferred as it directly yields the RI for the wavelengths of interest [56]. In any case, once the RI is known, the correction consists of a simple division of the measurement made on the image (the optical path) by the RI, which will result in the (correct) physical path.

The kinetic behavior of the t→m growth measured by SEM and OCT was similar, confirming that the opaque layer observed by OCT represents the same t→m layer observed by SEM. However, OCT measurements were not feasible for depths lower than ~5 μm. This is due to the axial resolution of the OCT system used in this study and the high reflectivity of the samples' surface. The OCT data of t→m transformation zone depth was used to calculate the ageing rate of 106 kJ/mol and 99.4 kJ/mol for infrastructure and monolithic, respectively.

According to the data of the linearity adjustment (r-square), the OCT presented a better fit compared with SEM (Fig. 10). The sample preparation procedures, and lower number of specimens may have influenced

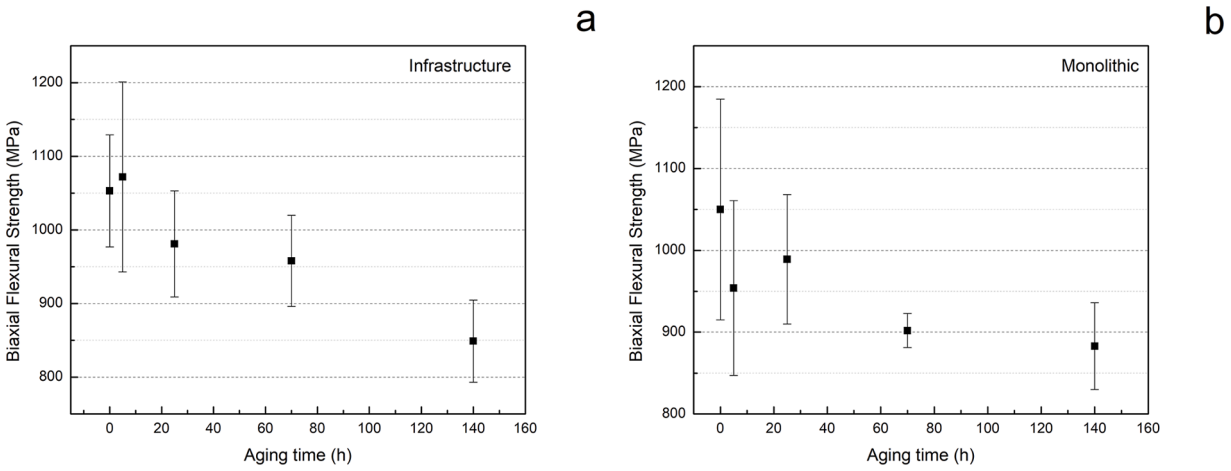

Fig. 11. Graphic showing the biaxial flexural mean (MPa) and respective standard deviation in comparison to the ageing time (h) in specimens hydrothermally aged at 150°C for the infrastructure (a) and monolithic (b) groups.

Table 4
Values of one-way ANOVA for flexural strength ($p < 0.05$) of the infrastructure ceramic.

	Source	df	SS	MS	F	p
Infrastructure	Hydrothermal ageing	4	313480	78370.05	11.25	<001*
	Error	45	314176	6981.68		
	Total	50	48957765			
Monolithic	Hydrothermal ageing	4	146031	36507.92	4.609	=0.01*
	Error	35	277230	7920.87		
	Total	40	37004701			

* Statistically significant difference at the level of 5%.

Table 5
Results of t→m phase (%), depth of the transformed zone (μm), flexural strength and respective standard deviation (MPa), respective confidence intervals (CI) of the infrastructure, and monolithic ceramic submitted to hydrothermal ageing at 150°C, 3.01 bar as a function of the ageing time, and lifetime estimation for a similar depth of the transformed zone at 37°C.

Ceramic	Ageing time	M phase %	Depth of the transformed zone (SEM)	Biaxial Flexural strength	Estimative EH 37°C**	
		(% t→m)	(μm)	(MPa)	SEM (year)	OCT (year)
Infrastructure (n=10)	0	0	0	1053^{ab}	-	-
	5	49.72	2.87	1072^{a}	41	35.9
	25	63.93	11.96	981^{ab}	170.8	149.5
	70	68.55	32.8	958^{b}	468.5	410
	140	65.8	62.67	849^{c}	895.2	783.3
Monolithic (n=8)	0	0	0	1059^{ab}	-	-
	5	50.36	-	954^{ac}	-	-
	25	64.61	5.83	989^{ab}	72.9	34.3
	70	64.64	46.76	902^{ac}	584.5	275
	140	67.14	85.55	883^{c}	1069.4	503.2

*Different lowercase letters indicate statistical difference among each ceramic group.
** Thickness estimation depth calculated in μm.

SEM results. Moreover, lower variations of the transformed layer depth obtained by SEM and OCT would propagate an exponential error resulting in different activation energy values, thus, different speed rates of the t→m transformed zone aged at 37°C.

The decrease of hardness and Young's modulus values, as well as the decrease in mechanical flexural strength, have a strong correlation with the increase of monoclinic phase [14,46,57]. The monolithic Y-TZP is also susceptible to LTD, and hardness and elastic modulus may be affected [12]. Premature failure of Y-TZP is related to microcracks and grain pullout from a damaged Y-TZP with high values of surface roughness [8,58,59]. Changes limited to Y-TZP surface caused by hydrothermal ageing are also reported in literature [60] However, the literature also shows studies demonstrating that t→m phase transformation of LTD Y-TZP did not decrease the material strength [13,16,61,62], and small periods of hydrothermal ageing time (5 h, 134°C) did not affect the Y-TZP hardness and fracture toughness [63]. Furthermore, an increase in Y-TZP strength after hydrothermal ageing have been described [53,64–66].

In this study, despite the high values of mechanical strength, both ceramics presented a decrease of strength after 140 h. of hydrothermal ageing at 150°C with a transformed layer depth of 62.67 μm (infrastructure Y-TZP) and 85.55 μm (monolithic Y-TZP) (Table 5). Twenty-

five and 70 h. of ageing resulted in t→m transformed zone depth of 12 μm and 32 μm, respectively, for the infrastructure zirconia. Similarly, for the monolithic zirconia, transformed layer depths of 5.8 μm (25 h. of ageing) and 46.7 μm (70 h. of ageing) did not affect flexural strength. According to the literature, the ageing time calculated for the biomedical Y-TZP (134°C for 5 h.) corresponds to 15–20 years of ageing at 37°C [67]. However, this result superestimates the ageing for the dental monolithic Y-TZP, where hydrothermal ageing of 134°C for 5 h. corresponded to 2-5 years at 37°C [12]. The variation of the results shows that the activation energy should be calculated to each Y-TZP material.

After initial ageing, it was possible to establish a negative correlation between the monoclinic phase content and mechanical strength of both Y-TZP materials. Microstructure, grain size, composition, sintering parameters, polishing procedures and density of the Y-TZP materials studied may have an effect on t→m transformation kinetics and on mechanical properties [7]. Divergences in literature concerning the strength of Y-TZP t→m phase transformation may be related to variations in the t→m transformation depth [68]. According to the results of the present study, it was possible to estimate that approximately 783 years (infrastructure) or 503 years (monolithic) of exposure at 37°C would be necessary for the materials to reach a level of t→m transformation that would lead to a significant decrease in flexural strength. However, these numbers do not take into account variations in pH, mechanical cycling, parafunctional habits and even bacteria colonization, challenges that are present in the oral environment and should be analyzed in future studies.

5. Conclusion

The findings of the present study indicate that:

- During hydrothermal ageing, there is a linear relationship between the thickness of the transformed layer and the ageing time observed by SEM and OCT.
- The sigmoidal behavior of the transformed layer is related to the penetration depth of the X-ray in the XRD technique.
- Y-TZP flexural strength is directly affected by the depth of the transformed layer. Infrastructure and monolithic zirconia presented 19.37% and 16.62% decrease in flexural strength after 140 h. of hydrothermal ageing at 150 °C, respectively.
- Based on the OCT results, the rate of Y-TZP transformed layer propagation at 37°C was calculated as 0.08 (±0.04) μm/year for both infrastructure and monolithic zirconia.
- OCT may be considered a reliable method to analyze Y-TZP t→m phase transformation kinetics upon hydrothermal ageing.

This conclusion concerns the specific dental Y-TZP materials tested in this study and may not be valid for other 3Y-TZP materials processed with different parameters, additives since the LTD is dependent of the ceramic microstructure.

Declaration of Competing Interest

The authors declare that they have no known competing financial interests or personal relationships that could have appeared to influence the work reported in this paper.

Acknowledgments

This manuscript was based on a doctorate thesis project done by the primary author, Anelyse Arata Found, with the title “Y-TZP dental ceramic low-temperature degradation: microstructural analysis and mechanical properties evaluation” at the Department of Materials Science and Technology Center, Nuclear and Energy Research Institute, IPEN-CNEN/SP, São Paulo University. The authors would like to thank Dr. Jian Wang from the laboratory of mechanical tests, Faculty of Dentistry, University of Toronto. The authors would like to thank MSc. Nildemar Aparecido Messias, Dr. Glauson Aparecido Ferreira and Dr. Larissa Otubo, Department of Materials Science and Technology Center, Nuclear and Energy Research Institute, IPEN-CNEN/SP for the scanning electron microscope imaging. This work was supported by a grant from the National Counsel of Technological and Scientific Development (CNPq: #162678/2012-6) and the Coordination for the Improvement of Higher Education Personnel (CAPES: #99999.008583/2014-05). The authors would like to thank the 3M-ESPE Canada for providing the Lava Plus blocks used in the study.

References

[1] A. Håff, H. Löf, J. Gunne, G. Sjögren, A retrospective evaluation of zirconia-fixed partial dentures in general practices: an up to 13-year study, Dent. Mater. 31 (2015) 162–170, https://doi.org/10.1016/j.dental.2014.11.009.
[2] V.C. Bachhav, M.A. Aras, Zirconia-based fixed partial dentures: a clinical review, Quintessence Int. 42 (2011) 173–182.
[3] Y. Zhang, B.R. Lawn, Novel Zirconia Materials in Dentistry, J. Dent. Res. 97 (2018) 140–147, https://doi.org/10.1177/0022034517737483.
[4] T.K. Gupta, F.F. Lange, J.H. Bechtold, Effect of stress-induced phase transformation on the properties of polycrystalline zirconia containing metastable tetragonal phase, J. Mater. Sci. 13 (1978) 1464–1470, https://doi.org/10.1007/BF00553200.
[5] R.C. Garvie, R.H. Hannik, R.T. Pascoe, Ceramic steel? Nature 258 (1975) 703–704, https://doi.org/10.1038/258703a0.
[6] R.H.J. Hannink, P.M. Kelly, B.C. Muddle, Transformation toughening in zirconia-containing ceramics, J. Am. Ceram. Soc. 83 (2004) 461–487, https://doi.org/10.1111/j.1151-2916.2000.tb01221.x.
[7] J. Chevalier, B. Cales, J. Drouin, Low temperature aging of Y-TZP ceramics, J. Am. Ceram. Soc. 82 (1999) 2150–2154. http://onlinelibrary.wiley.com/doi/10.1111/j.1151-2916.1999.tb02055.x/abstract. accessed April 29, 2014.
[8] M. Yoshimura, T. Noma, K. Kawabata, S. Sōmiya, Role of H_2O on the degradation process of Y-TZP, J. Mater. Sci. Lett. 6 (1987) 465–467, https://doi.org/10.1007/BF01756800.
[9] S. Deville, L. Gremillard, J. Chevalier, G. Fantozzi, A critical comparison of methods for the determination of the aging sensitivity in biomedical grade yttria-stabilized zirconia, J. Biomed. Mater. Res. B Appl. Biomater. 72B (2005) 239–245, https://doi.org/10.1002/jbm.b.30123.
[10] G.K.R. Pereira, A.B. Venturini, T. Silvestri, K.S. Dapieve, A.F. Montagner, F.Z. M. Soares, L.F. Valandro, Low-temperature degradation of Y-TZP ceramics: a systematic review and meta-analysis, J. Mech. Behav. Biomed. Mater. 55 (2016) 151–163, https://doi.org/10.1016/j.jmbbm.2015.10.017.
[11] P. Kohorst, L. Borchers, J. Strempel, M. Stiesch, T. Hassel, F. Bach, C. Hübsch, Low-temperature degradation of different zirconia ceramics for dental applications, Acta Biomater. 8 (2012) 1213–1220, https://doi.org/10.1016/j.actbio.2011.11.016.
[12] M. Cattani-lorente, S. Durual, M. Amez-Droz, H.W.A. Wiskott, S.S. Scherrer, Hydrothermal degradation of a 3Y-TZP translucent dental ceramic : a comparison of numerical predictions with experimental data after 2 years of aging, Dent. Mater. 32 (2015) 394–402, https://doi.org/10.1016/j.dental.2015.12.015.
[13] K.S. Dapieve, L. s F. Guilardi, T. Silvestri, M.P. Rippe, G.K.R. Pereira, L.F. Valandro, Mechanical performance of Y-TZP monolithic ceramic after grinding and aging: Survival estimates and fatigue strength, J. Mech. Behav. Biomed. Mater. 87 (2018) 288–295, https://doi.org/10.1016/j.jmbbm.2018.07.041.
[14] K. Furuya, S. Takemoto, S. Yamashita, H. Sekine, Y. Yajima, M. Yoshinari, Low-temperature degradation of high-strength Y-TZP (yttria-stabilized tetragonal zirconia polycrystal), Dent. Mater. J. (2020), https://doi.org/10.4012/dmj.2019-090.
[15] P.H.C.O. Prado, J.B. Monteiro, T.M.B. Campos, G.P. Thim, R.M. de Melo, Degradation kinetics of high-translucency dental zirconias: Mechanical properties and in-depth analysis of phase transformation, J. Mech. Behav. Biomed. Mater. 102 (2020), 103482, https://doi.org/10.1016/j.jmbbm.2019.103482.
[16] S. Wille, P. Zumstrull, V. Kaidas, L.K. Jessen, M. Kern, Low temperature degradation of single layers of multilayered zirconia in comparison to conventional unshaded zirconia: Phase transformation and flexural strength, J. Mech. Behav. Biomed. Mater. 77 (2018) 171–175, https://doi.org/10.1016/j.jmbbm.2017.09.010.
[17] V. Lughi, V. Sergo, Low temperature degradation -aging- of zirconia: a critical review of the relevant aspects in dentistry, Dent.Mater. 26 (2010) 807–820, https://doi.org/10.1016/j.dental.2010.04.006.
[18] M. Keuper, K. Eder, C. Berthold, K.G. Nickel, Direct evidence for continuous linear kinetics in the low-temperature degradation of Y-TZP, Acta Biomater. 9 (2013) 4826–4835, https://doi.org/10.1016/j.actbio.2012.08.032.
[19] J. Chevalier, J. Loh, L. Gremillard, S. Meille, E. Adolfson, Low-temperature degradation in zirconia with a porous surface, Acta Biomater. 7 (2011) 2986–2993, https://doi.org/10.1016/j.actbio.2011.03.006.
[20] F. Zhang, M. Inokoshi, K. Vanmeensel, B. Van Meerbeek, I. Naert, J. Vleugels, Lifetime estimation of zirconia ceramics by linear ageing kinetics, Acta Mater. 92 (2015) 290–298, https://doi.org/10.1016/j.actamat.2015.04.001.
[21] D. Huang, E.A. Swanson, C.P. Lin, J.S. Schuman, W.G. Stinson, W. Chang, M. R. Hee, T. Flotte, K. Gregory, C.A. Puliafito, Optical coherence tomography, Science 254 (1991) 1178–1181.

[22] A. Freitas, M. Amaral, M. Raele, F.J. Duarte, Optical coherence tomography: development and applications. Laser Pulse Phenomena and Applications, InTechOpen, Rijeka, 2010, pp. 409–432, https://doi.org/10.5772/12899.

[23] J.M. Schmitt, Optical coherence tomography (OCT): a review, IEEE Journal of Selected Topics in Quantum Electronics 5 (1999) 1205–1215.

[24] B. Bouma, G.J. Tearney, Handbook of Optical Coherence Tomography, CRC Press, 2001. https://books.google.ca/books?id=3r3zgdeO8XgC.

[25] M.A. and D.A.H. Izatt Joseph, A. Choma, J.G. Fujimoto, D. Wolfgang, Theory of optical coherence tomography. Optical Coherence Tomography: Technology and Applications, Springer International Publishing, Cham, 2015, pp. 65–94, https://doi.org/10.1007/978-3-319-06419-2_3.

[26] B.D. Cullity, S.R. Stock, Elements of X-Ray Diffraction, 3rd ed., Prentice Hall, New York, 2001.

[27] B.L. Henke, E.M. Gullikson, J.C. Davis, X-Ray interactions: photoabsorption, scattering, transmission, and reflection at E = 50-30,000 eV, Z = 1-92, At. Data Nucl. Data Tables 54 (1993) 181–342, https://doi.org/10.1006/adnd.1993.1013.

[28] R.A. Young, The Rietveld Method, Oxford University Press, New York, 1993.

[29] R.G. Mortimer, Physical Chemistry, 3rd ed., Elsevier Academic Press, New York, 2008.

[30] International Organization for Standardization, Dentistry- Ceramic Materials (ISO Standard No. 6872:2008), 2008.

[31] I. Sailer, B.E. Pjetursson, M. Zwahlen, C.H.F. Hämmerle, A systematic review of the survival and complication rates of all-ceramic and metal-ceramic reconstructions after an observation period of at least 3 years. Part II: fixed dental prostheses, Clin. Oral Implant. Res. 18 (2007) 86–96, https://doi.org/10.1111/j.1600-0501.2007.01468.x.

[32] M.V Swain, Unstable cracking (chipping) of veneering porcelain on all-ceramic dental crowns and fixed partial dentures, Acta Biomater. 5 (2009) 1668–1677, https://doi.org/10.1016/j.actbio.2008.12.016.

[33] B. Stawarczyk, M. Özcan, F. Schmutz, A. Trottmann, M. Roos, C.H.F. Hämmerle, Two-body wear of monolithic, veneered and glazed zirconia and their corresponding enamel antagonists, Acta Odontol. Scand. 71 (2013) 102–112, https://doi.org/10.3109/00016357.2011.654248.

[34] Y. Zhang, J.J.W. Lee, R. Srikanth, B.R. Lawn, Edge chipping and flexural resistance of monolithic ceramics, Dent. Mater. 29 (2013) 1201–1208, https://doi.org/10.1016/j.dental.2013.09.004.

[35] Y. Zhang, Making yttria-stabilized tetragonal zirconia translucent, Dent. Mater. 30 (2014) 1195–1203, https://doi.org/10.1016/j.dental.2014.08.375.

[36] J. Klimke, M. Trunec, A. Krell, Transparent tetragonal yttria-stabilized zirconia ceramics: influence of scattering caused by birefringence, J. Am. Ceram. Soc. 94 (2011) 1850–1858, https://doi.org/10.1111/j.1551-2916.2010.04322.x.

[37] E. Camposilvan, R. Leone, L. Gremillard, R. Sorrentino, F. Zarone, M. Ferrari, J. Chevalier, Aging resistance, mechanical properties and translucency of different yttria-stabilized zirconia ceramics for monolithic dental crown applications, Dent. Mater. 34 (2018) 879–890, https://doi.org/10.1016/j.dental.2018.03.006.

[38] Y. Xiong, Z. Fu, V. Pouchly, K. Maca, Z. Shen, Preparation of Transparent 3Y-TZP Nanoceramics with No Low-Temperature Degradation, J. Am. Ceram. Soc. 97 (2014) 1402–1406, https://doi.org/10.1111/jace.12919.

[39] G. Pekkan, K. Pekkan, B.Ç. Bayindir, M. Özcan, B. Karasu, Factors affecting the translucency of monolithic zirconia ceramics: A review from materials science perspective, Dent. Mater. J. 39 (2020) 1–8, https://doi.org/10.4012/dmj.2019-098.

[40] H. Zhang, Z. Li, B. Kim, K. Morita, H. Yoshida, K. Hiraga, Y. Sakka, Effect of Alumina Dopant on Transparency of Tetragonal Zirconia, J. Nanomater. (2012) 1–5, https://doi.org/10.1155/2012/269064.

[41] J. Chevalier, L. Gremillard, S. Deville, Low-temperature degradation of zirconia and implications for biomedical implants, Ann. Rev. Mater. Res. 37 (2007) 1–32, https://doi.org/10.1146/annurev.matsci.37.052506.084250.

[42] J. Chevalier, S. Grandjean, M. Kuntz, G. Pezzotti, On the kinetics and impact of tetragonal to monoclinic transformation in an alumina/zirconia composite for arthroplasty applications, Biomaterials 30 (2009) 5279–5282, https://doi.org/10.1016/j.biomaterials.2009.06.022.

[43] P. Fabbri, C. Piconi, E. Burresi, G. Magnani, F. Mazzanti, C. Mingazzini, Lifetime estimation of a zirconia–alumina composite for biomedical applications, Dent. Mater. 30 (2014) 138–142, https://doi.org/10.1016/j.dental.2013.10.006.

[44] W.A. Johnson, R.F. Mehl, Reaction kinetics in processes of nucleation and growth, Trans. Am. Inst. Min. Metall. Petrol. Eng. 135 (1939) 416–441.

[45] L. Gremillard, J. Chevalier, T. Epicier, S. Deville, G. Fantozzi, Modeling the aging kinetics of zirconia ceramics, J. Eur. Ceram. Soc. 24 (2004) 3483–3489, https://doi.org/10.1016/j.jeurceramsoc.2003.11.025.

[46] M. Cattani-Lorente, S.S. Scherrer, P. Ammann, M. Jobin, H.W.A. Wiskott, Low temperature degradation of a Y-TZP dental ceramic, Acta Biomater. 7 (2011) 858–865, https://doi.org/10.1016/j.actbio.2010.09.020.

[47] L. Gremillard, S. Grandjean, J. Chevalier, A new method to measure monoclinic depth profile in zirconia-based ceramics from X-ray diffraction data, Int. J. Mater. Res. (2010).

[48] H. Yang, Y.L. Xu, G. Hong, H. Yu, Effects of low-temperature degradation on the surface roughness of yttria-stabilized tetragonal zirconia polycrystal ceramics: A systematic review and meta-analysis, J. Prosthet. Dent. (2020) 1–9, https://doi.org/10.1016/j.prosdent.2020.01.005.

[49] R. Garvie, P. Nicholson, Phase analysis in zirconia systems, J. Am. Ceram. Soc. 55 (1972) 303–305.

[50] A. Arata, T.M.B. Campos, J.P.B. Machado, D.R.R. Lazar, V. Ussui, N.B. Lima, R. N. Tango, Quantitative phase analysis from X-ray diffraction in Y-TZP dental ceramics: A critical evaluation, J. Dent. 42 (2014) 1487–1494, https://doi.org/10.1016/j.jdent.2014.08.010.

[51] M.J. Starink, On the meaning of the impingement parameter in kinetic equations for nucleation and growth reactions, J. Mater. Sci. 36 (2001) 4433–4441, https://doi.org/10.1023/A:1017974517877.

[52] S. Ban, Chemical durability of high translucent dental zirconia, Dent. Mater. J. 39 (2020) 12–23, https://doi.org/10.4012/dmj.2019-109.

[53] G.K.R. Pereira, M. Amaral, P.F. Cesar, M.C. Bottino, C.J. Kleverlaan, L.F. Valandro, Effect of low-temperature aging on the mechanical behavior of ground Y-TZP, J. Mech. Behav. Biomed. Mater. 45 (2015) 183–192, https://doi.org/10.1016/j.jmbbm.2014.12.009.

[54] G.Q.M. Monteiro, M.A.J.R. Montes, A.S.L. Gomes, C.C.B.O. Mota, S.L. Campello, A. Z. Freitas, Marginal analysis of resin composite restorative systems using optical coherence tomography, Dent. Mater. 27 (2011) e213–e223, https://doi.org/10.1016/j.dental.2011.08.400.

[55] C. Sampaio, R. Rodrigues, E. Souza-Junior, A. Freitas, G. Ambrosano, F. Pascon, R. Puppin-Rontani, Effect of restorative system and thermal cycling on the tooth-restoration, Interface OCT Eval. Oper. Dent. 41 (2016) 162–170, https://doi.org/10.2341/14-344-L.

[56] L.R. de Pretto, M.M. Amaral, A.Z. de Freitas, M.P. Raele, Nondestructive evaluation of fused filament fabrication 3D printed structures using optical coherence tomography, Rapid Prototyp. J. 26 (2020) 1853–1860, https://doi.org/10.1108/RPJ-12-2019-0314.

[57] B.D. Flinn, D.A. DeGroot, L.A. Mancl, A.J. Raigrodski, Accelerated aging characteristics of three yttria-stabilized tetragonal zirconia polycrystalline dental materials, J. Prosthet. Dent. 108 (2012) 223–230, https://doi.org/10.1016/S0022-3913(12)60166-8.

[58] T. Sato, M. Shimada, Crystalline phase change in yttria-partially-stabilized zirconia by low-temperature annealing, J. Am. Ceram. Soc. 67 (1984), https://doi.org/10.1111/j.1151-2916.1984.tb19668.x. C-212-C–213.

[59] J. Chevalier, What future for zirconia as a biomaterial? Biomaterials 27 (2006) 535–543, https://doi.org/10.1016/j.biomaterials.2005.07.034.

[60] L. Borchers, M. Stiesch, F. Bach, J. Buhl, C. Hübsch, T. Kellner, P. Kohorst, M. Jendras, Influence of hydrothermal and mechanical conditions on the strength of zirconia, Acta Biomater. 6 (2010) 4547–4552, https://doi.org/10.1016/j.actbio.2010.07.025.

[61] G.K.R. Pereira, C. Muller, V.F. Wandscher, M.P. Rippe, C.J. Kleverlaan, L. F. Valandro, Comparison of different low-temperature aging protocols: its effects on the mechanical behavior of Y-TZP ceramics, J. Mech. Behav. Biomed. Mater. 60 (2016) 324–330, https://doi.org/10.1016/j.jmbbm.2016.02.017.

[62] H. Papanagiotou, S. Morgano, R.A. Giordano, R. Pober, In vitro evaluation of low-temperature aging effects and finishing procedures on the flexural strength and structural stability of Y-TZP dental ceramics, J. Prosthet. Dent. Prosthet. Dent. 96 (2006) 154–164.

[63] K. Harada, A. Shinya, H. Gomi, Y. Hatano, A. Shinya, A.J. Raigrodski, Effect of accelerated aging on the fracture toughness of zirconias, J. Prosthet. Dent. 115 (2016) 215–223, https://doi.org/10.1016/j.prosdent.2015.08.020.

[64] S. Deville, J. Chevalier, L. Gremillard, Influence of surface finish and residual stresses on the ageing sensitivity of biomedical grade zirconia, Biomaterials 27 (2006) 2186–2192, https://doi.org/10.1016/j.biomaterials.2005.11.021.

[65] M. Inokoshi, K. Vanmeensel, F. Zhang, J. De Munck, G. Eliades, S. Minakuchi, I. Naert, B. Van Meerbeek, J. Vleugels, Aging resistance of surface-treated dental zirconia, Dent. Mater. 31 (2015) 182–194, https://doi.org/10.1016/j.dental.2014.11.018.

[66] M. Amaral, L.F. Valandro, M.A. Bottino, R.O.A. Souza, Low-temperature degradation of a Y-TZP ceramic after surface treatments, J. Biomed. Mater. Res. Part B 101B (2013) 1387–1392, https://doi.org/10.1002/jbm.b.32957.

[67] J. Chevalier, J.M. Drouin, B. Cales, Low temperature ageing behavior of zirconia hip joint heads, Bioceramics 10 (1997) 135–138.

[68] K. Wongkamhaeng, D.V. Dawson, J.A. Holloway, I. Denry, Effect of surface modification on in-depth transformations and flexural strength of zirconia ceramics, Journal of Prosthodontics 28 (2019) e364–e375, https://doi.org/10.1111/jopr.12908.